FEM Modeling and Simulation of 2-D High Specific Heat Nb_3Sn Wires

Fermilab 2019 - *Summer Student*: Fabrizio Berritta
Supervisor: Alexander Zlobin, *Co-supervisor*: Emanuela Barzi.

In the past few years, new high specific heat Nb_3Sn wires have gained much focus at FNAL. Indeed, they have proved to be more stable against thermal perturbations with respect to standard wires. Nevertheless, a trade off exists between their thermal efficiency and production feasibility. In this report I describe the thermal and structural models that I have developed by exploiting ANSYS Mechanical APDL®, which I got acquainted with at the beginning of my training. The aim has been to optimize the location of high specific heat elements in order to obtain an optimal thermal stability, while minimizing the risk of wire breakage during drawing. FEM results are compared with experimental ones made beforehand. Other minimum quench energy (MQE) thermal models have been developed for expected new experimental results. New data may improve the understanding of the embedded physical uncertainties in the model.

I. Introduction

Nb_3SN magnets are known to require longer training than other magnets. In general, the first quench (i.e. transition from superconducting to normal phase) occurs at 60-70% of the short sample limits and more than 20 quenches are required to reach the magnet nominal field [1]. However, higher critical currents are required to fulfill the needs of higher magnetic fields, leading to greater instability issues that must be treated carefully in order to reduce cost and magnet test time during the training. Indeed, as training quenches are performed a gradual improvement of the magnet's performance occurs until the plateau establishes.

It is known that quenches of Nb_3Sn magnets are determined by thermal perturbations caused by conductor motion (e.g. due to Lorentz forces), epoxy cracking etc. These thermal perturbations results in a local thermal heating of the wire that could eventually make the wire phase change to the normal state. In an adiabatic model the minimum quench energy (MQE) is simply defined as the integration of the conductor's specific heat over the temperature margin within the superconducting state. The idea, which dates back to 1960, is to reduce the MQE by inserting high specific heat (H-C_p) elements in the wire [2].

In this introduction, focus on Nb_3Sn, quenching and Finite-Element-Method (FEM) is provided. The second and third sections discuss the thermal and structural 2-D analysis, respectively. They have been realized by means of the commercial FEM program ANSYS Mechanical APDL®. The thermal analysis is compared with experimental results taken from [1]. On the other hand, the outcomes from the plastic simulation are discussed considering the geometry of an actual H-C_p wire that was broken during drawing. Other models waiting for experimental results and the commented scripts have not been included in this report, but provided to the supervisors.

A. Nb_3Sn and Composite Wires

The energy of a circular collider is limited by the strength of the bending dipole magnets. This explains why higher-field accelerator magnets have gained much attention by High Energy Physics (HEP) and Particle Accelerator communities [3]. Even though the highest fields have been obtained exploiting superconducting electromagnets, the maximum nominal field of NbTi accelerator magnets is not high enough anymore. At the moment the Large Hadron Collider (LHC), at the European Organization for Nuclear Research (CERN, Switzerland), is limited to $\sim 8\,\mathrm{T}$ at $1.9\,\mathrm{K}$.

Fermi National Accelerator Laboratory, which operated one of the largest SC accelerators in the world, the Tevatron, is pushing beyond the NbTi LHC magnets by exploring superconductors with higher critical parameters. Considering the present state-of-the-art Nb_3Sn wires, a $\sim 50\%$ improvement of the critical current density (J_c) is also required for $16\,\mathrm{T}$ dipoles [4]. Nb_3Sn is an inter metallic type II superconductor with critical temperature $T_{c0} = 18.3\,\mathrm{K}$ and B_{c20} up to $30\,\mathrm{T}$. For comparison, NbTi has a T_{c0} of $9.3\,\mathrm{K}$ and B_{c20} of $15\,\mathrm{T}$. Still, the major drawbacks of Nb_3Sn are its brittleness due to the high-temperature processing and its critical current being strain sensitive, which is to say superconductivity may be lost because of sufficiently high strain.

To obtain the required current in the cable, several strands are connected in parallel and twisted or transposed along the axial direction. The strands in the cable are not insulated from each other for letting the current redistribute in the case of localized defects or quenches [3]. Mainly, thin superconducting filaments are positioned in a normal low resistance matrix to assure better stability with respect to flux jumps and further protection in case of quenching. An example of the 150/169 wire cross section is shown in Fig. 1. The number 150 refers to the number of superconducting strands in the wire, whereas 169 is the maximum value that could be achieved without the internal Cu hexagon. The main advantages of the copper matrix are the high thermal conductivity and the high specific heat. The former enhances heat transportation away from the filaments, while the latter promotes absorption of a

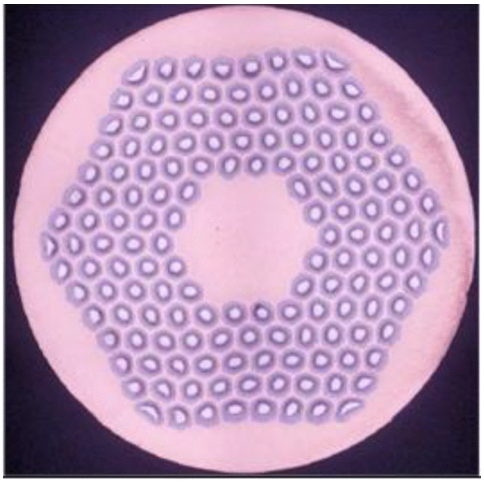

Fig. 1. Cross section of 150/169 Nb3Sn wire of the Restacked Rod Process® type [5]. The matrix is made of Cu, whereas the 150 hexagonal Nb_3Sn sub-elements contain bronze.

large fraction of heat and it decreases Joule heating as the superconductor loses its superconductor capability. Induced eddy currents by time-dependent fields are reduced by twisting the filaments; this solution also improves stability to flux jumps.

B. Quench Origins and H-C_p Elements Implementation

The previously mentioned critical current, temperature and magnetic field define a *critical surface* within which the superconducting state is sustained, i.e. non measurable resistivity and perfect diamagnetism. In general a magnet operates below the critical surface, but as soon as the current is being ramped up one gets closer to the critical surface. Crossing it means that a small volume V switches to the normal resistive state. Power is therefore dissipated by means of Joule effect, leading to a temperature increase of the surrounding volume dV. If the temperature reached by dV approaches the critical temperature, then further power is dissipated and the process keeps going by means of thermal diffusion. The normal zone propagates through the entire coil and the magnet quenches.

Two different kinds of quench mechanism are defined: *conductor-limited* and *energy-deposited* quenches [6]. In order to distinguish them, it is assumed a conductor of known critical current $I_c(T, B)$. Actually, the maximum magnetic field seen by the conductor is a function of the current itself $B = f(I)$, resulting in the following implicit equation for the maximum current I_{max}:

$$I = I_c(T_0, f(I)) \qquad \text{at } T_0.$$

If the quench occurs at I_{max} then it is due to the intrinsic properties of the conductor: it is a *conductor-limited* quench. The other kind of quench occurs at a current I lower than $I_{max}(T_0)$, since in a volume of the coil the temperature has been raised to $T_0 + \Delta T$, such that

$$I \geq I_c(T_0, f(I)) \quad .$$

These quenches are *energy-deposited* since they take place because of an energy deposit.

Hence, in conductor-limited quenches the critical surface is crossed because of a *current* increase, whereas in the energy-deposited quenches the critical surface is crossed due to a local *temperature* increase. In the following, I will consider only the latter since they are the cause of magnet training. Furthermore, the magnetic field B will be assumed to be solely the external one fixed by the experimental setup.

As mentioned in the previous page, it is possible to increase the minimum quench energy (MQE) by adding H-C_p substances. At Fermilab a design compatible with high-J_c multifilamentary Nb_3Sn wires [1] has been formulated. Some Nb_3Sn sub-elements have been substituted by Cu tubes filled with H-C_p powders. However, they have been mixed with Cu powder to counteract their low thermal diffusivity that would otherwise preclude heat diffusion from the outer Cu matrix into the H-C_p strands. It is known that Gd_2O_3 has an high specific heat at low temperatures; e.g. the monoclinic structure shows a peak at $3.8\,\mathrm{K}$ [7]. The optimal position of these H-C_p in terms of thermal efficiency should be intuitively at the outermost layer of the Nb_3Sn, in order to shield those sub-elements from external perturbations. Unfortunately, it has not been possible to realize this structure because of wire breakage during drawing in the past. Different configurations have been realized, as discussed in the second section.

C. Thermal Analysis Discretization by Finite Element Method

Since the optimization of a model lies its ground on the apprehending of both underlying physical and numerical methods, before tackling the physical aspect it is important to outline how a FEM works, at least in a linear case.
Starting from the *strong formulation*, i.e. the PDE to be solved, we want to derive the associated *weak formulation* that can be solved numerically, with the inevitable approximations. We define the *Sobolev spaces* $H^k(\Omega), k \geq 1$, and $H^k(\Omega)$ contains all the functions $f(\mathbf{r})$ such that their partial derivatives of total order $\leq k$ are square-integrable in Ω. For $k = 0$ we have $H^0(\Omega) = L^2(\Omega)$, where $L^2(\Omega)$ is the vector space of all square-integrable functions in the domain $\Omega \subset \mathbb{R}^2$. Its associated norm is defined as:

$$\|f\|_{H^k} = \left(\sum_{0 \leq i+j \leq k} \int_\Omega \left| \frac{\partial^{i+j} f}{\partial x_1^i \partial x_2^j} \right|^2 d\mathbf{x} \right)^{1/2} \quad , \quad k \geq 0 \quad .$$

Considering the 2-D case with a piece-wise smooth domain boundary Γ with no cusps, it can be proved that all the elements of $H^2(\Omega)$ are continuous functions on $\overline{\Omega}$ (the domain including its boundary), while $H^1(\Omega)$ includes also non continuous functions [8]. By defining $c_p(\mathbf{r})$ the temperature-independent specif heat capacity per unit volume of conductor $(\mathrm{J\,m^{-3}})$, $\mathbf{K}(\mathbf{r})$ a second-order tensor whose components are the thermal conductivity coefficients $(\mathrm{W\,m^{-1}\,K^{-1}})$ and P_r is the Joule heating rate per unit volume $(\mathrm{W\,m^{-3}})$ the heat balance equation follows [6]:

$$c_p(\mathbf{r}) \frac{\partial T(\mathbf{r}, t)}{\partial t} = \nabla \cdot (\mathbf{K}(\mathbf{r}) \nabla T(\mathbf{r}, t)) + P_r(\mathbf{r}, t) \quad . \qquad (1)$$

In the following we drop the position dependency for ease of notation. Moreover, since our model is a 2-D one, the system is invariant along the axial (z) direction and in the following the constant units are modified accordingly. As we shall see, ANSYS sets an unitary thickness in 2-D models. Therefore, assuming that the enclosed functions are sufficiently smooth, it is possible to rewrite (1) for the 2-D model in:

$$\begin{cases} c_p\,\dot{T}(t) = \nabla\cdot(\mathbf{K}\,\nabla T(t)) + P_r(t), & \text{in } \Omega,\ 0 < t \le T \\ T(0) = T_0, & \text{in } \overline{\Omega}, \\ T(\mathbf{r},t) = T_{\text{env}}, & \text{on } \Gamma,\ 0 < t \le T, \end{cases} \tag{2}$$

where the boundary conditions of the starting temperature T_0 and the temperature constraint T_{env} of the environment at the boundary Γ at all times have been set. Both T_0 and T_{env} are constants; (2) is the starting *strong formulation*. In order to derive the associated *weak formulation*, we have to apply Green's formula for the divergence. Foremost, we have to define the vector space of our *test functions* $V = H^1_\Gamma(\Omega) = \{v(\mathbf{r}) \in H^1(\Omega) \mid v(\Gamma) = 0\}$; then the previous equation is multiplied by $v \in V$ and all terms are integrated over the domain Ω. It results:

$$\begin{cases} \displaystyle\int_\Omega c_p\dot{T}(t)v\,d\mathbf{x} - \int_\Omega \nabla\cdot(\mathbf{K}\,\nabla T(t))v\,d\mathbf{x} = \\ \qquad \displaystyle= \int_\Omega P_r(t)v\,d\mathbf{x}, \quad \forall v \in V,\ 0 < t \le T, \\ T(0) = T_0, \quad \text{in } \overline{\Omega}, \\ T(t) = T_{\text{env}}, \quad \text{on } \Gamma,\ 0 < t \le T\,. \end{cases}$$

Then, we apply the Green's formula for the divergence. Now the *weak formulation* takes the following form: *for any given* t, $0 < t \le T$, *find* $T(t) \in W = H^1(\Omega)$ such that

$$\begin{cases} \displaystyle\int_\Omega c_p\dot{T}(t)v\,d\mathbf{x} + \int_\Omega \mathbf{K}\,\nabla T(t)\cdot\nabla v\,d\mathbf{x} = \\ \qquad \displaystyle= \int_\Omega P_r(t)v\,d\mathbf{x}, \quad \forall v \in V, 0 < t \le T \\ T(0) = T_0, \quad \text{in } \overline{\Omega}, \\ T(t) = T_{\text{env}}, \quad \text{on } \Gamma,\ 0 < t \le T\,. \end{cases}$$

The latter can be rewritten in a more concise form as:

$$\begin{cases} \left(\dot{T}(t), v\right) + a\left(T(t), v\right) = \left(P_r(t), v\right), \quad \forall v \in V, \\ T(0) = T_0, \quad \text{in } \overline{\Omega}, \\ T(t) = T_{\text{env}}, \quad \text{on } \Gamma,\ 0 < t \le T\,. \end{cases} \tag{3}$$

where the inner product is the integral of the product of two functions over Ω and the bi-linear form

$$a\left(T(t), v\right) = \int_\Omega \mathbf{K}\,\nabla T(t)\cdot\nabla v\,d\mathbf{x}$$

has been defined. For each $0 < t \le T$ the previous weak formulation has a unique solution $T(t) \in H^1(\Omega)$.

In order to apply the FEM, in the following it is assumed that the domain Ω has a polygonal boundary. In this case, it is possible to define a discretization $\{K_m\}$, where K_m denotes a generic element of the mesh. For simplicity we consider a triangular mesh with interior nodes x_i being labeled from 1 to N_h, while the boundary nodes go from N_h+1 to N_t. Then it is chosen $V_h = span\{\varphi_j,\ j = 1 : N_h\} \subset W$ where $\varphi_j(x_i) = \delta_{ij}$ are the chosen basis functions, as depicted for example in Fig. 2. Analogously, $W_h = span\{\varphi_j,\ j = 1 : N_t\} \subset V$ and $T(t)$ is substituted by $T_h(t)$. At this point $\forall v_h \in V_h$ is equivalent to $\forall \varphi_i,\ i = 1 : N_h$, because of linearity. The problem in the new (spatial) discretization is to find $T_t(t) \in W_h$ such that:

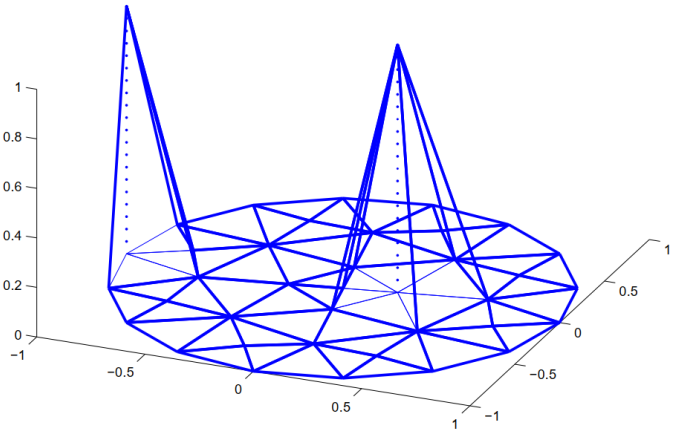

Fig. 2. 2D piece-wise linear FEM basis functions. At a boundary node (left) and at internal node (right) [9].

$$\begin{cases} \left(\dot{T}_h(t), \varphi_i\right) + a(T_h(t), \varphi_i) = (P_r(t), \varphi_i),\ i = 1 : N_h \\ T_h(0) = T_0, \qquad \forall x_j \text{ with } j = 1 : N_t, \\ T_h(x_j, t) = T_{\text{env}}, \qquad j = N_{h+1} : N_t,\ 0 < t \le T\,. \end{cases}$$

From the hypothesis $T_h(t) \in W_h$, it is set:

$$T_h(t)(\mathbf{r}) = \sum_{j=1}^{N_t} c_j(t)\varphi_j(\mathbf{r}), \quad 0 \le t \le T$$

Recalling the property of the basis $\varphi_i(x_j) = \delta_{ij}$, by applying the boundary condition at $t = 0$ and $t > 0$, we obtain, respectively:

$$c_j(0) = T_0,\ \forall x_j \text{ with } j = 1 : N_t, \tag{4}$$

$$c_j(t) = T_{\text{env}},\ \forall x_j \text{ with } j = N_{h+1} : N_t,\ 0 < t \le T\,. \tag{5}$$

Therefore, for $t > 0$, the coefficients $\{c_j(t),\ j = 1 : N_h\}$ are the solutions of the following system of ODEs:

$$\begin{cases} \displaystyle\sum_{j=1}^{N_h} \dot{c}_j(t) \underbrace{\int_\Omega \varphi_j\varphi_i d\mathbf{x}}_{m_{ij}} + \sum_{j=1}^{N_h} c_j(t) \underbrace{a\left(\varphi_j, \varphi_i\right)}_{a_{ij}} = \\ \displaystyle= \underbrace{\int_\Omega P_r(t)\varphi_i d\mathbf{x} - \sum_{j=N_h+1}^{N_t} T_{\text{env}}\, a\left(\varphi_j, \varphi_i\right)}_{d_i}, \quad i = 1 : N_h \\ c_j(0) = T_0,\ j = 1 : N_t. \end{cases} \tag{6}$$

Therefore, the system can be written as

$$\begin{cases} \mathbf{M}\dot{\mathbf{c}}(t) + \mathbf{A}\mathbf{c}(t) = \mathbf{d}(t) \\ \mathbf{c}(0) = \mathbf{u}_0 \end{cases} \tag{7}$$

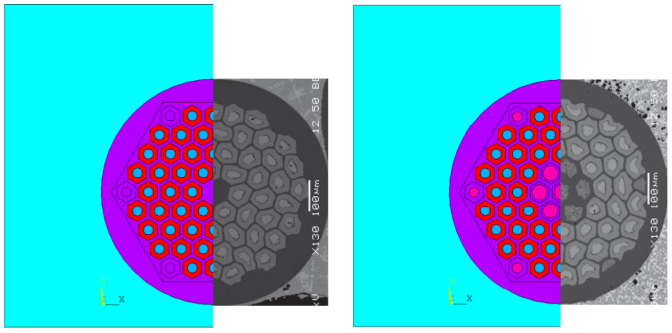

Fig. 3. Hypertech geometries of (left) normal wire and (right) High-C_p wires, both having $0.7\,\mathrm{mm}$ diameter.

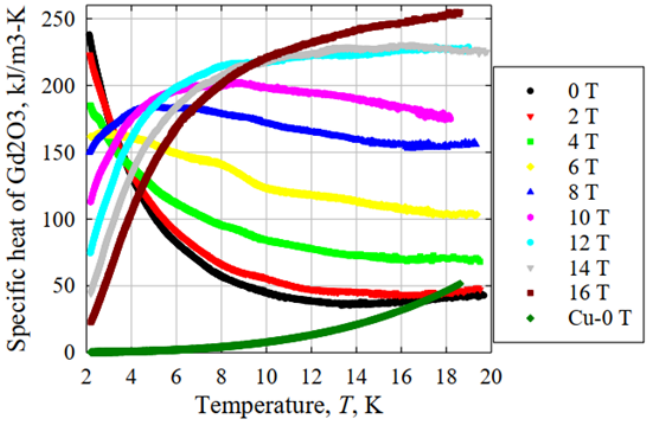

Fig. 4. measured specific heat of Gd_2O_3. X. Xu, A. V. Zlobin, E. Barzi – Fermilab; C. Buehler, M. Field, B. Sailer, M. Wanior, H. Miao – Bruker EST; C. Tarantini – Florida State University. "*Enhancing specific heat of Nb3Sn conductors to improve stability and reduce training*". Presented at CEC-ICMC 2019.

where both $\mathbf{M}$ (the *mass matrix*) and $\mathbf{A}$ are highly sparse. The first order linear ODE system is a *semi-discretization* since only space and not time has been discretized. The latter can be discretized by common numerical methods. It is important to emphasize that this FEM has been applied to a linear heat transfer equation. The ANSYS model, being the material properties dependent on temperature, is strictly non-linear and iterative algorithms are required to obtain a solution with the required accuracy. The interested reader may find more information in [10].

II. Thermal Analysis

In the following, two different kinds of wires have been simulated. The firsts have been produced by *Hypertech* and the others by *Bruker*. The former High-C_p version contained Gd_2O_3 sub-elements in the innermost row and at the six corners of a $0.7\,\mathrm{mm}$ diameter wire. Its experimental results served to test the validity of the relative model. On the contrary, the High-C_p Bruker wire contained the high capacity components in the outermost row and its drawing process failed at the diameter of about $4\,\mathrm{mm}$. The Bruker geometry has been chosen to understand how the position and the number of Gd_2O_3 sub-elements affected the wire efficiency against thermal perturbation. At the moment no experimental results are available for the Bruker wires. The chosen element type has been PLANE55 and the mesh was sufficiently refined until no changes occurred in the second decimal digit of the wires maximum temperatures after the heat pulse.

A. Hypertech Wires

The 61-restack Hypertech wires described in [1] have been modeled in 2-D as depicted in Fig. 3. The normal wire is surrounded by the stycast which acts as a thermal insulator, whereas the Nb_3Sn sub-elements are embedded in a copper matrix. The Nb_3Sn hexagons contain bronze due to the fabrication process and six-corners of Nb_3Sn have been replaced by copper. On the other hand, the High-C_p contains seven Gd_2O_3 sub-elements at the center and at the six corners. The wire is not at the center of the stycast to better represent the experimental setup, therefore half the model has been realized because of symmetry with respect to the $\hat{y}$ direction. Our reference system is assumed to be centered at the wire center, with the axes parallel to the ones depicted in the previous figure. Regarding the geometrical lengths:

- wire diameter $0.7\,\mathrm{mm}$;
- bronze rods radius $15\,\mu\mathrm{m}$;
- sub-elements width $2 \cdot 29/\sqrt{3}\,\mu\mathrm{m}$;
- thickness between two sub-elements $10\,\mu\mathrm{m}$;
- stycast, total width W_{sty} and height H_{sty} are $1.3\,\mathrm{mm}$ and $1.0\,\mathrm{mm}$, respectively. It has been displaced along y by $(H_{sty} - R_{wire})/8$;
- Gd_2O_3 sub-elements radius $23\,\mu\mathrm{m}$ (only in High-C_p wire).

The chosen material properties as a function of temperature are fully described in Appendix A. The effect of the applied magnetic field, $B = 12\,\mathrm{T}$, is considered only in the copper thermal conductivity and Gd_2O_3 specific heat. All the Gd_2O_3 properties have been mixed with the copper ones to consider the powder mixture, as described in the introduction. The standard linear rule of mixture has been chosen, with Cu : Gd_2O_3= 1 : 2. It is interesting to notice in Fig. 4 that the peaked behaviour of [7] specific heat is lost as magnetic fields are applied. Nonetheless, the specif heat of Gd_2O_3 remains sufficiently high as experimental results have shown.

The next step has been the choice of the thermal load to simulate a MQE experiment. In [1] a flat strain gage has been applied on top of the wire and the energy has been obtained by integrating over time the dissipated power due to Joule heating effect in the gage. Being the FEM model a 2-D one, a *thermal flux* impinging on a circumference arc has been chosen, corresponding to $\theta \in [90°, 120]°$. Being half the model, this means that the heat flux has been applied to $30° \cdot 2/360° = 1/6$ of the wire circumference in the full model. It will be shown that the choice of θ changes the results by small percentages. As boundary condition, the initial temperature is set to be $T_0 = 4.2\,\mathrm{K}$ because of the helium bath, whereas at the boundaries $T_{\mathrm{env}} = 4.2\,\mathrm{K}$ is kept fixed. Along $x = 0$ no boundary conditions have been

applied, resulting in an adiabatic setting for ANSYS. The latter is required to model half the model, since no heat flux occurs along that line because of the problem symmetry.

The heat flux pulse period has been set to $200\,\mu s$ and its amplitude has been evaluated by dividing the input energy by two, the pulse period and the area. The factor of two derives from modelling half the wire, whereas the area is just the arc length upon which the flux is applied multiplied by an unitary width, that is the thickness dimension used by ANSYS in 2-D models [10]. At this point we are interested in obtaining the MQE as a function of the normalized transport current I/I_c. While in the experimental setup the current is the input and the MQE is measured, in this FEM model their roles are exchanged. However, in the FEM simulation no currents are available, just the maximum temperature of the wire is. The idea has been to consider the maximum temperature, at given input energy, as the critical temperature associated to the required critical current. Therefore the following empirical relationship for Nb_3Sn has been used [12]:

$$I_c(B,T) = \frac{C(\varepsilon)}{\sqrt{B}}\left[1-\frac{B}{B_{c2}(T,\varepsilon)}\right]^2\left[1-\left(\frac{T}{T_{c0}}\right)^2\right]^2 \quad , \tag{8}$$

where

$$C(\varepsilon) = \frac{I_{REF}(\varepsilon)\sqrt{12\,\mathrm{T}}}{\left[1-\frac{12\,\mathrm{T}}{B_{c2}(4.2\,\mathrm{K},\varepsilon)}\right]^2\left[1-\left(\frac{4.2\,\mathrm{K}}{T_{c0}(\varepsilon)}\right)^2\right]^2} \quad , \tag{9}$$

and

$$\frac{B_{c2}(T,\varepsilon)}{B_{c20}(\varepsilon)} = \left[1-\left(\frac{T}{T_{c0}(\varepsilon)}\right)^2\right]\times$$
$$\times\left\{1-0.31\left(\frac{T}{T_{c0}(\varepsilon)}\right)^2\left[1-1.77\ln\left(\frac{T}{T_{c0}(\varepsilon)}\right)\right]\right\} \tag{10}$$

The already fitted parameters $I_{ref} = 489\,\mathrm{A}$, $T_{c0} = 16.96\,\mathrm{K}$ and $B_{c20} = 27.89\,\mathrm{T}$ have been chosen, considering null strain $\varepsilon = 0$. Therefore, the critical current $I_{c0} = I_c(12\,\mathrm{T},\,4.2\,\mathrm{K})$ has been obtained and considering the maximum temperature of the wire as T_c, the current ratio $\tilde{I}_{T_c} = I_c(12\,\mathrm{T}, T_c)/I_{c0}$ has been evaluated for each heat flux pulse. As an order of magnitude for Nb_3Sn at $12\,\mathrm{T}$, critical temperatures of $6.3\,\mathrm{K}$ and $4.4\,\mathrm{K}$ correspond to critical current ratios of 0.2 and 0.8, respectively.

The simulation results are presented in Fig. 5 and they are compared with experimental ones. It can be appreciated that the ratio of the MQE is almost three times in both the simulation and the experimental data. Therefore, the thermal model has well reproduced the thermal efficiency of the high specific heat wires. Nonetheless, the curves are lower then the acquired data. Even though (8) is an approximated fitting expression, the major difference is given by how the heat has been applied by the strain gage. Indeed, heat conduction occurs in all direction in the experiment, whereas in the simulation the heat flux has been directed towards the wire

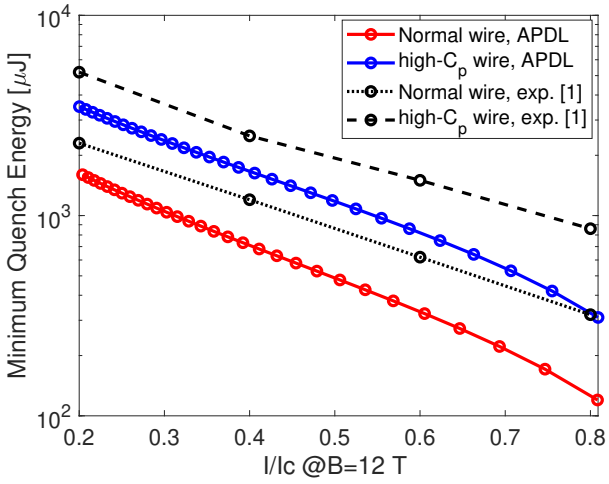

Fig. 5. Hypertech wire, comparison between MQE simulations and experiment [1].

itself. Therefore, the required heat required in the simulation to reach a certain temperature is lower than the experimental one. Moreover, if one were interested in an absolute model rather than relative, also the minimum propagation zone (MPZ) should be considered. Indeed, an energy deposited quench occurs only if the local increase in temperature occurs beyond a given volume V_0 inside the wire. A 1-D treatment of the problem can be found in [13]. From a qualitative point of view, since the strain gage was $\sim 4\,\mathrm{mm}$ long while in the ANSYS model unitary thickness is assumed, the required heat in the laboratory would be higher considering the MPZ effect.

In order to study the sensitivity of the model with respect to the chosen material properties, the FEM has been tested several times, changing the specific heat or thermal conductivity of one material separately. Each material property has been changed by $\pm 20\%$, whose value has been selected in order to obtain appreciable differences in some plots. The results are summarized in Tab. I, II. In the tables, "Dev." stands for 'Deviation' and in the same row are indicated how $\tilde{I}_{T_c,\alpha_i=\pm 20\%}$ changes from $\tilde{I}_{T_c}$, where $\alpha_i = \pm 20\%$ represents the material property changed by $\pm 20\%$ at all temperatures. It resulted that for each material changes, the minimum deviation (in absolute value) from the original simulation occurs at the lowest MQE and vice versa for the largest. It is interesting to note that Nb_3Sn specific heat has the greatest impact on the normal wire final temperature, whereas the high-C_p is strongly dependent on the Gd_2O_3 specific heat.

Last, it resulted that the previously defined thermal load θ changes $\tilde{I}_{T_c}$ by about 5% at most, as described in Tab. III. From the latter it can be noticed that smaller angles result in lower current ratio values. This behaviour has been explained by considering the heating more localized for small angles, resulting in lower dissipation towards the stycast and slightly higher increase in the wire temperature.

TABLE I
MATERIAL SENSITIVITY NORMAL WIRE FOR THERMAL SIMULATION.

Thermal conductivity	Min. Dev. [%]	MQE Min. Dev. [µJ]	Max. Dev. [%]	MQE Max. Dev. [mJ]
Stycast: $\Delta\kappa = -20\%$	-1.4	$3.2{\cdot}10^2$	-3.5	$2.3{\cdot}10^3$
Stycast: $\Delta\kappa = 20\%$	1.2	$3.2{\cdot}10^2$	3.3	$2.3{\cdot}10^3$
Cu: $\Delta\kappa = -20\%$	-0.15	$3.2{\cdot}10^2$	-0.63	$2.3{\cdot}10^3$
Cu: $\Delta\kappa = 20\%$	0.11	$3.2{\cdot}10^2$	0.46	$2.3{\cdot}10^3$
Nb_3Sn: $\Delta\kappa = -20\%$	-0.060	$3.2{\cdot}10^2$	-0.27	$2.3{\cdot}10^3$
Nb_3Sn: $\Delta\kappa = 20\%$	0.050	$3.2{\cdot}10^2$	0.21	$2.3{\cdot}10^3$
Bronze: $\Delta\kappa = -20\%$	<0.01	$3.2{\cdot}10^2$	<0.01	$2.3{\cdot}10^3$
Bronze: $\Delta\kappa = 20\%$	<0.01	$3.2{\cdot}10^2$	<0.01	$2.3{\cdot}10^3$
Specific heat	Min. Dev. [%]	MQE Min. Dev. [µJ]	Max. Dev. [%]	MQE Max. Dev. [mJ]
Stycast: $\Delta c_p = -20\%$	-1.1	$3.2{\cdot}10^2$	-3.0	$2.3{\cdot}10^3$
Stycast: $\Delta c_p = 20\%$	0.97	$3.2{\cdot}10^2$	2.8	$2.3{\cdot}10^3$
Cu: $\Delta c_p = -20\%$	-1.7	$3.2{\cdot}10^2$	-4.9	$2.3{\cdot}10^3$
Cu: $\Delta c_p = 20\%$	1.6	$3.2{\cdot}10^2$	4.8	$2.3{\cdot}10^3$
Nb_3Sn: $\Delta c_p = -20\%$	-3.7	$3.2{\cdot}10^2$	-9.7	$2.3{\cdot}10^3$
Nb_3Sn: $\Delta c_p = 20\%$	3.3	$3.2{\cdot}10^2$	9.3	$2.3{\cdot}10^3$
Bronze: $\Delta c_p = -20\%$	-0.32	$3.2{\cdot}10^2$	-0.76	$2.3{\cdot}10^3$
Bronze: $\Delta c_p = 20\%$	0.32	$3.2{\cdot}10^2$	0.76	$2.3{\cdot}10^3$

TABLE II
MATERIAL SENSITIVITY HIGH-C_p WIRE FOR THERMAL SIMULATION.

Thermal conductivity	Min. Dev. [%]	MQE Min. Dev. [µJ]	Max. Dev. [%]	MQE Max. Dev. [mJ]
Stycast: $\Delta\kappa = -20\%$	-0.54	$8.6{\cdot}10^2$	-2.0	$5.2{\cdot}10^3$
Stycast: $\Delta\kappa = 20\%$	0.50	$8.6{\cdot}10^2$	1.9	$5.2{\cdot}10^3$
Cu: $\Delta\kappa = -20\%$	-0.42	$8.6{\cdot}10^2$	-1.5	$5.2{\cdot}10^3$
Cu: $\Delta\kappa = 20\%$	0.31	$8.6{\cdot}10^2$	1.1	$5.2{\cdot}10^3$
Nb_3Sn: $\Delta\kappa = -20\%$	-0.18	$8.6{\cdot}10^2$	-0.62	$5.2{\cdot}10^3$
Nb_3Sn: $\Delta\kappa = 20\%$	0.14	$8.6{\cdot}10^2$	0.50	$5.2{\cdot}10^3$
Bronze: $\Delta\kappa = -20\%$	<0.01	$8.6{\cdot}10^2$	-0.010	$2.3{\cdot}10^3$
Bronze: $\Delta\kappa = 20\%$	<0.01	$8.6{\cdot}10^2$	0.010	$5.2{\cdot}10^3$
Gd_2O_3: $\Delta\kappa = -20\%$	-0.020	$8.6{\cdot}10^2$	-0.050	$5.2{\cdot}10^3$
Gd_2O_3: $\Delta\kappa = 20\%$	0.010	$8.6{\cdot}10^2$	0.050	$5.2{\cdot}10^3$
Specific heat	Min. Dev. [%]	I/Ic Min. Dev. [µJ]	Max. Dev. [%]	I/Ic Max. Dev. [mJ]
Stycast: $\Delta c_p = -20\%$	-0.45	$8.6{\cdot}10^2$	-1.8	$5.2{\cdot}10^3$
Stycast: $\Delta c_p = 20\%$	0.41	$8.6{\cdot}10^2$	1.7	$5.2{\cdot}10^3$
Cu: $\Delta c_p = -20\%$	-0.73	$8.6{\cdot}10^2$	-3.1	$5.2{\cdot}10^3$
Cu: $\Delta c_p = 20\%$	0.72	$8.6{\cdot}10^2$	3.1	$5.2{\cdot}10^3$
Nb_3Sn: $\Delta c_p = -20\%$	-1.4	$8.6{\cdot}10^2$	-5.5	$5.2{\cdot}10^3$
Nb_3Sn: $\Delta c_p = 20\%$	1.3	$8.6{\cdot}10^2$	5.3	$5.2{\cdot}10^3$
Bronze: $\Delta c_p = -20\%$	-0.12	$8.6{\cdot}10^2$	-0.41	$5.2{\cdot}10^3$
Bronze: $\Delta c_p = 20\%$	0.12	$8.6{\cdot}10^2$	0.42	$5.2{\cdot}10^3$
Gd_2O_3: $\Delta c_p = -20\%$	-5.6	$8.6{\cdot}10^2$	-13	$5.2{\cdot}10^3$
Gd_2O_3: $\Delta c_p = 20\%$	4.8	$8.6{\cdot}10^2$	14	$5.2{\cdot}10^3$

B. Bruker Wires

In the following the Bruker wire has been modeled, as depicted in Fig. 6. The wire drawing failed at approximately $4\,\mathrm{mm}$ diameter, almost one order of magnitude larger than the aimed $0.7\,\mathrm{mm}$ final diameter. Therefore, the structure with the

TABLE III
LOAD ANGLE SENSITIVITY FOR THERMAL SIMULATION. THE ANGLE REFERS TO THE FEM MODEL, THUS $\theta \in [0, 180]^\circ$. THE ORIGINAL ANGLE IN SIMULATIONS IS 30°.

Normal wire	Min. Dev. [%]	MQE Min. Dev. [µJ]	Max. Dev. [%]	MQE Max. Dev. [mJ]
$\Delta\theta = -20^\circ$	-0.45	$3.2{\cdot}10^2$	-2.0	$2.3{\cdot}10^3$
$\Delta\theta = -10^\circ$	-0.14	$3.2{\cdot}10^2$	-0.64	$2.3{\cdot}10^3$
$\Delta\theta = 10^\circ$	0.14	$3.2{\cdot}10^2$	0.58	$2.3{\cdot}10^3$
$\Delta\theta = 20^\circ$	0.26	$3.2{\cdot}10^2$	1.1	$2.3{\cdot}10^3$
High c_p wire	Min. Dev. [%]	MQE Min. Dev. [µJ]	Max. Dev. [%]	MQE Max. Dev. [mJ]
$\Delta\theta = -20^\circ$	-1.3	$8.6{\cdot}10^2$	-4.6	$5.2{\cdot}10^3$
$\Delta\theta = -10^\circ$	-0.49	$8.6{\cdot}10^2$	-1.8	$5.2{\cdot}10^3$
$\Delta\theta = 10^\circ$	0.37	$8.6{\cdot}10^2$	1.4	$5.2{\cdot}10^3$
$\Delta\theta = 20^\circ$	0.68	$8.6{\cdot}10^2$	2.5	$5.2{\cdot}10^3$

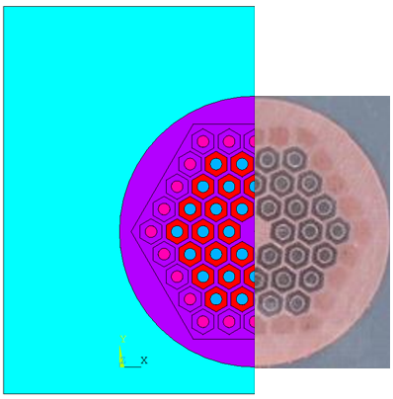

Fig. 6. Bruker geometry of High-C_p wire, diameter $1.91\,\mathrm{cm}$.

Gd_2O_3 components in the outermost row has not been realized yet. The reason for trying this pattern is that structures with Gd_2O_3 at the external row should shield the inner wire more efficiently against thermal perturbations. The aim has been to verify this hypothesis. Differently from the previous geometry, the high-C_p sub-elements in the model have the same area as the bronze rods. In addition to the previous high specific heat wire with 24 sub-elements (full model) of Gd_2O_3 in Fig. 6, six FEM models have been simulated:

- normal wire;
- 6 high-C_p sub-elements in the innermost row;
- 6 high-C_p sub-elements at the six corners of the external hexagon;
- 24 high-C_p sub-elements in the first two innermost rows and six corners;
- 18 high-C_p sub-elements in the first two innermost rows;
- 20 high-C_p sub-elements randomly positioned.

The MQE simulations are presented in Fig. 7. It is important to outline that two pairs of curves having the same number of Gd_2O_3:Cu sub-elements mixture overlap each other. The first overlapping is due to the total number of 6, whereas the other occurs in the 24 case. Therefore FEM simulations have shown that the number of these components has a much greater impact then their location. Actually, the curves having the Gd_2O_3 components far from wire center are slightly more efficient. Nonetheless, the mechanical feasibility of high specific heat wires has seemed to decrease as these brittle high-specific heat components are inserted further away from the wire center. Thus, the simulations have shown that it is possible develop new structures without worrying about thermal efficiency as long as the number of high-C_p sub-elements remains sufficiently high.

III. STRUCTURAL ANALYSIS

In parallel with the thermal simulations, structural models have been realized by using element type PLANE-182. Since the Bruker wire broke during the drawing process at about $4\,\mathrm{mm}$ diameter, new structural models have been been developed to predict the drawing failure. Regarding the load, an inward radial displacement of the wire has been chosen. Radial displacement has been selected instead of applying a pressure load on the wire because of in-homogeneous wire shrinking in the second case. The in-homogeneity was due to the internal hexagonal disposition of the sub-elements. Since the wire has been correctly drawed to $1.91\,\mathrm{cm}$ diameter, assuming simply zero strain in the given structure, the radial displacement decreased the diameter length to $1.81\,\mathrm{cm}$, about 5%. Higher values led to stress and strain contour plots with no appreciable differences between different materials in the wire and they were discarded.

The FEM structural geometry is shown with the corresponding results in Fig. 8. The material properties are listed in A. Since the drawing process is before the annealing process, the 'normal' sub-elements are made of niobium with tin in the central rods, as Nb_3Sn and bronze are obtained after the thermal treatment. The FEM simulation clearly shows that the gadolinium mixture with copper has higher stress when it is positioned in the outermost layer. The same occurs for the copper surrounding these structures, even though the colour scale is not sufficiently sensible to appreciate the differences in the copper stress at the center of the wire. Unfortunately the color scale could not be made more precise because of the software setting and the difference in the two cases are not sufficient to tell whether the wire may break or not. Several contour plots of stress, strain and plastic work

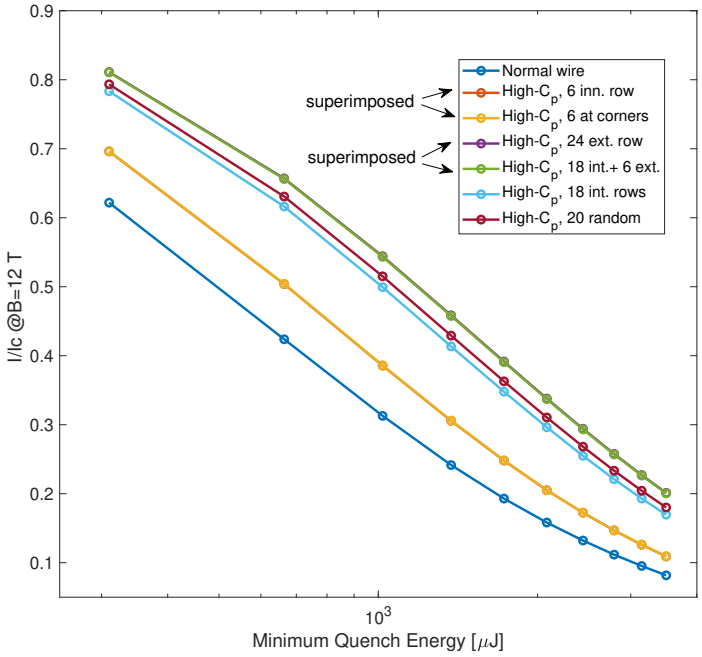

Fig. 7. Thermal simulation of Bruker geometry with different high specific heat sub-elements location and number.

have been realized for nine structural models. In some cases higher stress results in the normal wire configuration. Hence, further analyses are required and they have not been performed because of not sufficient time.

IV. Conclusion

Several 2-D FEM thermal models have been developed in order to study the MQE of Nb_3Sn superconducting wires. The developed relative model has been verified with the experimental results performed on the Hypertech wires [1]. Afterwards, it has been discovered that the position of the high-specif heat sub-elements has a negligible contribution regarding the thermal efficiency of the wire. Being their number most important against thermal perturbation, the constrain of thermal efficiency is relaxed because of a greater freedom in new structures development. This result increases the mechanical feasibility of these high-specific heat wires. New experimental data are expected from the normal Bruker wire. Regarding the structural model, further analyses are required to find the right criteria that would predict the wire drawing failure.

Appendix A
Material Properties

A. Thermal properties

In Tab. IV are listed the material properties for the thermal analyses; the Nb_3Sn ones refers to the superconducting state. The values have been evaluated by several fitting expressions:

- Nb_3Sn: thermal conductivity [15] (at 15 T not 12 T because not present), specific heat [14];
- Cu: thermal conductivity and specific heat from [14], linear fit for the former;
- Bronze: Sn [wt %] =5.46 [16]; the specific heat has been fitted linearly.
- Stycast: thermal conductivity [17] (linear fit) and specific heat [18];
- Gd_2O_3: thermal conductivity [19], specific heat from Fig. 4.

B. Structural properties

The mechanical properties are summarized in Tab. V. The values of the elastic modulus have been taken from https://www.engineeringtoolbox.com/, except the Gd_2O_3 from https://www.azom.com/. Different sources have been used for the real stress vs strain curves:

- Nb, [20];
- Cu, from https://www.copper.org (oxygen free copper);
- Sn, [21];
- Gd_2O_3, [22].

References

[1] X. Xu, A. V. Zlobin, X. Peng and P. Li, "*Development and Study of Nb3Sn Wires With High c_p ,*" in IEEE Transactions on Applied Superconductivity, vol. 29, no. 5, pp. 1-4, Aug. 2019, Art no. 6000404.
[2] R. Hancox, "*Enthalpy stabilized superconducting magnets*," IEEE Trans. Magn., vol. MAG-4, no. 3, pp. 486–488, Sep. 1968.
[3] E. Barzi and A. V. Zlobin, "*Research and Development of* Nb_3Sn *Wires and Cables for High-Field Accelerator Magnets,*" in IEEE Transactions on Nuclear Science, vol. 63, no. 2, pp. 783-803, April 2016.
[4] X. Xu, "*A review and prospects for Nb3 Sn superconductor development,*" Supercond. Sci. Technol., vol. 30, no. 9, 2017, Art. no. 093001.
[5] M. B. Field et al., "*Optimizing conductors for high field applications,*" IEEE Trans. Appl. Supercond, vol. 24, no. 3, p. 6001105, Jun. 2014.
[6] A. Devred, "*Quench Origins*,", KEK Report 89-25, March 1990.
[7] R. W. Hill et al., "*The c_p s of LaAg, GdAg and Gd2O3 from 0.5 to 22K*," Journal of Physics C: Solid State Physics, Volume 16, Number 15.

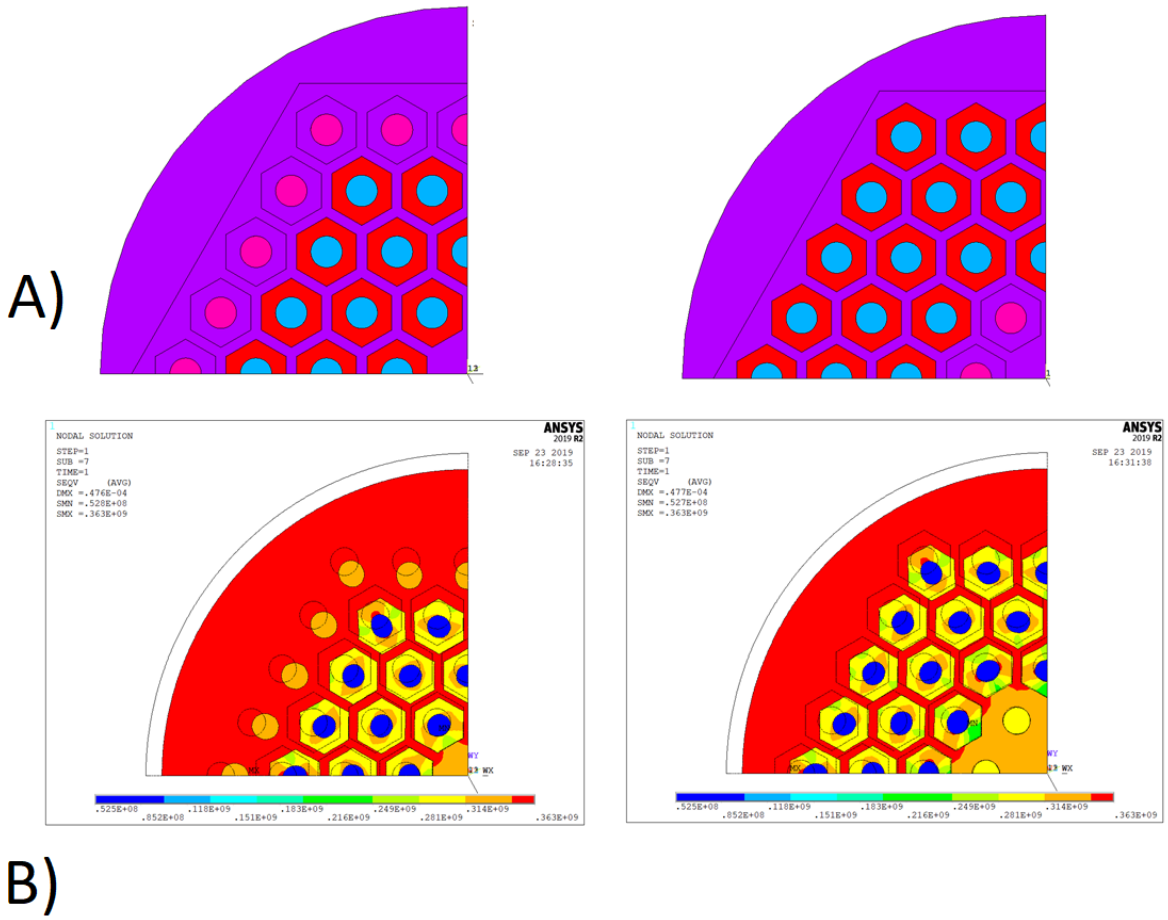

Fig. 8. Top, Bruker wire geometries for structural simulation. Bottom, Von Mises real stress expressed in Pa.

TABLE IV
MATERIAL PROPERTIES FOR THERMAL SIMULATION: THERMAL CONDUCTIVITY κ $\left[\mathrm{W\,m^{-1}\,K^{-1}}\right]$, SPECIFIC HEAT c_p $\left[\mathrm{J\,kg^{-1}\,K^{-1}}\right]$ AND MATERIAL DENSITY.

	Nb_3Sn (SC) $[8400\,\mathrm{kg\,m^{-3}}]$		Cu $[8960\,\mathrm{kg\,m^{-3}}]$		Bronze $[8850\,\mathrm{kg\,m^{-3}}]$		Stycast $[2400\,\mathrm{kg\,m^{-3}}]$		Gd_2O_3 $[7410\,\mathrm{kg\,m^{-3}}]$	
Temp.	κ	c_p	κ	c_p	κ	c_p	κ	c_p	κ	c_p
4 K	174	0.409	158	0.0911	1.9	0.129	0.07	0.44	6.2	22
6 K	237	0.935	237	0.226	2.9	0.194	0.11	1.7	6.2	27
8 K	308	1.85	315	0.470	3.9	0.387	0.15	3.7	6.2	29
10 K	320	3.27	394	0.856	4.9	0.968	0.19	6.2	6.2	29

TABLE V
MATERIAL PROPERTIES FOR STRUCTURAL SIMULATION. THE HIGHLIGHTED ONES HAVE BEEN IMPLEMENTED IN ANSYS.

Material	**Elastic modulus** [GPa]	**Poisson ratio**	Ultimate tensile strength [MPa]	Yield strength [MPa]
Nb	103	0.40	95	50.0
Sn	47.0	0.36	(15:200)	10.0
Cu	124	0.34	334	320
Gd_2O_3	55.0	0.26	170	200

[8] A. Quarteroni, "*Numerical Models for Differential Problems,*" 2nd edition, Springer Publishing Company, 2013.
[9] G. Monegato, "*Notes on Finite Element Modeling,*", lecture notes AY. 2018/2019.
[10] M. K. Thompson and J. M. T., "*ANSYS Mechanical APDL for Finite Element Analysis,*" 1st edition, Butterworth-Heinemann, 2017.

[11] X. Xu, P. Li, A. V. Zlobin and X. Pen,"*Improvement of stability of Nb3Sn superconductors by introducing high specific heat substances,*" in IOP, Supercond. Sci. Technol., 31 (2018), 03LT02.

[12] Barzi E.,Turrioni D., "*Short sample limit calculation for 1 m long dipole MBHSP02 made of 150/169 RRP® strand and cored cable* " Fermilab, Batavia, IL, USA, Tech. Note, TD-00-041, 2000.

[13] A. Stenvall, A. Korpela, J. Lehtonen, R. Mikkonen, *"Formulation for solving 1D minimum propagation zones in superconductors"*, Physica C: Superconductivity and its Applications, Volume 468, Issue 13, 2008, Pages 968-973.

[14] G. Manfreda, C. Barbagallo, *"Review of ROXIE's Material Properties Database for Quench Simulation"*, CERN, Magnets, Superconductors and Cryostats TE-MSC Internal Note 2018-1178007.

[15] Bonura, M., and C. Senatore. "*Thermal Conductivity of Industrial* Nb_3Sn *Wires Fabricated by Various Techniques.*" IEEE Transactions on Applied Superconductivity 23.3 (2013): 6000404–6000404. Crossref. Web.

[16] N.J. Simon, E.S. Drexler and R.P. Reed, "Properties of Copper and Copper Alloys at Cryogenic Temperatures", NIST Monography 177, Ed.1992.

[17] F.Rondeaux, Ph.Bredy and J.M.Rey, "Thermal Conductivity Measurements of Epoxy Systems at Low Temperatures", I-01C-02, Poster presented at Cryogenic Engineering Conference (CEC), July 16-20, 2001 Madison, Wisconsin, USA.

[18] Swenson, C.A., *Linear thermal expansivity (1.5–300 K) and heat capacity (1.2–90 K) of Stycast 2850FT*, Review of Scientific Instruments, 1997.

[19] Dargis, Rytis & Williams, D & Smith, R & Arkun, F. Erdem & Roucka, Radek & Clark, Andrew & Lebby, Michael. (2012). *Structural and Thermal Properties of Single Crystalline Epitaxial Gd2O3 and Er2O3 Grown on Si(111)*. ECS Journal of Solid State Science and Technology. 1. N24. 10.1149/2.005202jss.

[20] H. S. Kim , "Analysis of materials properties of niobium tube from the results of a virtual bulge test", AIP Conference Proceedings 1435, 305 (2012).

[21] Hotta, Satoshi & Matsumoto, Keigo & Murakami, Taichi & Narushima, Takayuki & Ouchi, Chiaki. (2007). *Dynamic and Static Restoration Behaviors of Pure Lead and Tin in the Ambient Temperature Range*. MATERIALS TRANSACTIONS. 48. 2665-2673.

[22] D. S. Petrovic et al, "Microstructural Anisotropy of Magnetocaloric Gadolinium Cylinders: Effect on the Mechanical Properties of the Material", Materials (Basel). 2016 May; 9(5): 382.